Journal of Physics G: Nuclear and Particle Physics

PAPER • **OPEN ACCESS**

True muonium resonant production at e^+e^- colliders with standard crossing angle

To cite this article: Ruben Gargiulo *et al* 2024 *J. Phys. G: Nucl. Part. Phys.* **51** 045004

OPEN ACCESS
IOP Publishing
Journal of Physics G: Nuclear and Particle Physics
J. Phys. G: Nucl. Part. Phys. **51** (2024) 045004 (18pp)
https://doi.org/10.1088/1361-6471/ad2974

True muonium resonant production at e^+e^- colliders with standard crossing angle

Ruben Gargiulo[1], Stefano Palmisano[1], Elisa Di Meco[2], Eleonora Diociaiuti[2], Ivano Sarra[2] and Daniele Paesani[3]

[1] Università degli Studi La Sapienza, Piazzale Aldo Moro 5, I-00185 Roma, Italy
[2] INFN Laboratori Nazionali di Frascati, Via Enrico Fermi 54, I-00044 Frascati, Italy
[3] Università degli Studi di Roma Tor Vergata, Via della Ricerca Scientifica 1, I-00133 Roma, Italy

E-mail: ruben.gargiulo@lnf.infn.it

Received 3 October 2023, revised 4 February 2024
Accepted for publication 14 February 2024
Published 4 March 2024

Abstract

True muonium (TM) ($\mu^+\mu^-$) is the heaviest and smallest bound state not containing hadrons, after TM ($\tau^+\tau^-$) and mu-tauonium ($\mu^\pm\tau^\mp$). One of the proposed methods to observe the spin 1 fundamental state of TM, which has the smallest lifetime among TM spin 1 states, was to build an e^+e^- collider with a large crossing angle ($\theta \sim 30°$) in order to provide TM with a large boost and detect its decay vertex in e^+e^-. The following paper will instead show that TM excited states can be observed in relatively large quantities ($\mathcal{O}(10)$/month) at a e^+e^- collider with standard crossing angle, after setting their center-of-mass energy to the TM mass ($\sim 2m_\mu = 211.4$ MeV).

Keywords: particle physics, true muonium, QED bound states, precision frontier

1. Introduction

Quantum electrodynamics (QED) predicts the existence of several bound states, in addition to standard atoms, such as purely leptonic systems. Given the absence of clear signals beyond the Standard Model (BSM), precision measurements of QED bound states might be employed as new physics probes. However, observable quantities of bound states containing hadrons

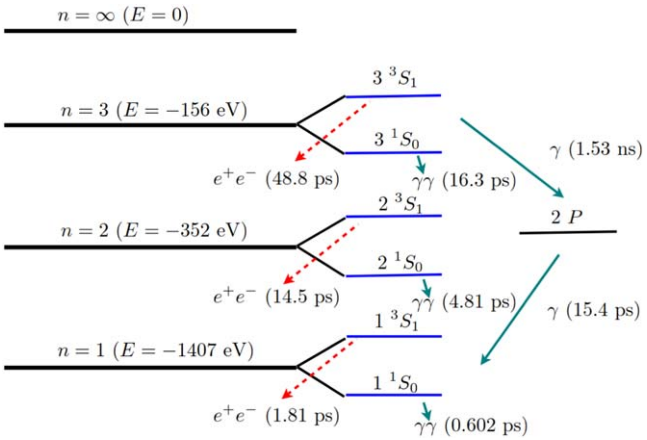

Figure 1. True muonium levels, lifetimes and transitions diagram for $n \leqslant 3$ (spacing not to scale) [12].

have large theoretical uncertainties from unknown non-perturbative quantum chromodynamics effects, while the properties of purely leptonic bound states (such as positronium [1]) can be calculated very precisely. At the same time, purely leptonic bound states containing electrons are limited in their BSM discovery potential through atomic spectroscopy by the mass suppression due to the small term $m_e/\Lambda_{\mathrm{BSM}}$. In contrast, bound states containing only μ and τ particles have much larger reduced masses so their BSM sensibility is enhanced [2]. One of the possible bound-state choices is represented by the so-called true muonium (TM), a bound state containing a μ^+ and a μ^-, that, with its 211.4 MeV mass and 512 fm Bohr radius constitutes the heaviest and smallest purely leptonic QED atom right after true tauonium ($\tau^+\tau^-$) [3] and mu-tauonium ($\mu^\pm\tau^\mp$).

It should be noted that addressing the search for BSM signals to muons is reasonable because of the long-standing 'muon problem': the coincidence that multiple observables in the muonic sector deviate from either theoretical predictions or similar results with other leptonic flavours [4]. TM precision measurements are also useful to the Standard Model itself, in the hypothesis of the absence of new physics at accessible scales, because its hyperfine splitting shifts are directly sensible to contributions from hadronic vacuum polarization [5], like for the muon anomalous magnetic moment [6].

It is interesting to point out that the ($\mu^+\mu^-$) bound state is called 'TM' since the name 'muonium' was previously used for the μ^+e^- bound state. Indeed, the first studies of TM only began as its production was shown to be feasible. Positronium and muonium have been observed and studied, while TM has not been observed yet.

Several production mechanisms have been proposed for TM, including meson decays, like $\eta \to TM\gamma$ [7, 8] and $K_L \to TM\gamma$ [9], or electron-nucleus $eZ \to e\,TM\,Z$ [10], nucleus-nucleus $Z_1Z_2 \to Z_1Z_2\,TM$ [11] and electron–positron $e^+e^- \to TM(\gamma)$ [12] collisions. This work focuses on the last method.

2. TM properties

The TM energy levels can be calculated by rescaling the positronium spectrum: the binding energy of the deepest level (1S) was evaluated to be B.E. (1S) = 1.4 keV, as shown in figure 1.

Like positronium, TM has two spin states: para-TM (spin 0), which decays to $\gamma\gamma$, and orto-TM (spin 1), which decays to e^+e^-.

For each of the two spin states, spontaneous transitions from the $(n+1)S/P$ to the nP/S are possible. While for S states these transitions compete with the decay, for P states they are mandatory. Indeed, the ortho-P states have $P = (-1)^{l\,+\,1\,=\,2} = 1$ and $C = (-1)^{l\,+\,s\,=\,1\,+\,1\,=\,2} = 1$, so they cannot annihilate to e^+e^- via a photon in the s-channel as the S states because of parity and charge conjugation conservation. The lifetimes of the nth S levels for the two spin states $s = 0$, 1 are proportional to n^3 (at lowest order), as follows:

$$\tau(nS_{s=1} \to e^+e^-) = \frac{6\hbar n^3}{\alpha^5 m_\mu c^2} \sim n^3 \times 1.8\ \text{ps} \tag{1}$$

$$\tau(nS_{s=0} \to \gamma\gamma) = \frac{1}{3}\tau(nS_{s=1} \to e^+e^-). \tag{2}$$

These lifetimes are much smaller than the muon lifetime, therefore the muons inside TM can be assumed as stable particles.

3. TM production in e^+e^- collisions

Once known the main TM characteristics, it is possible now to focus on its production methods. The most abundant processes to produce TM from e^+e^- collisions are: off-resonance $e^+e^- \to \text{TM}\,\gamma$ interactions at $\sqrt{s} > 2m_\mu$ with a hard recoil photon, and resonant $e^+e^- \to \text{TM}$ interactions at $\sqrt{s} \sim 2m_\mu$ [12]. Off-resonance interactions have a cross-section of:

$$\sigma_{\text{OFF}\,R.} \sim \frac{\pi}{2}\left[\ln\left(\frac{1+c_0}{1-c_0}\right) - c_0\right]\frac{\alpha^6}{s}, \tag{3}$$

where c_0 is the cosine of the detector acceptance polar angle, while resonant interactions have a much larger cross-section of:

$$\sigma_{\text{ON}\,R.} = 2\pi^2\frac{\alpha^3}{s} = \frac{\pi^2\alpha^3}{2m_\mu^2} = 66.6\ \text{nb}. \tag{4}$$

It must be pointed out that the probability to produce TM in a state n is proportional to n^{-3} [12], and the normalization factor is $\zeta(3)$, where:

$$\zeta(k) = \sum_{n=1}^{+\infty}\frac{1}{n^k} \tag{5}$$

is the Riemann Zeta function.

For TM production at colliders, the cross-section in equation (4) is reduced accounting for the the probability p that the beam center-of-mass energy is in the energy window $(m_\mu - B.E.(1S),\ m_\mu)$ where bound states are allowed [12].

Considering that the energy window width $\Delta E = B.E.(1S) = 1.4$ keV is much smaller than the beam's energy spread σ_E, for a Gaussian distribution this p factor is simply given by the peak value of the $\sqrt{s}$ probability density function (where $\sigma_{\sqrt{s}} = \sqrt{2}\,\sigma_E$) multiplied by ΔE, namely

$$p = \frac{\Delta E}{2\sqrt{\pi}\sigma_E} = \frac{\Delta E}{2\sqrt{\pi}m_\mu}\left(\frac{\sigma_E}{E}\right)^{-1} = 3.7 \times 10^{-6}\left(\frac{\sigma_E}{E}\right)^{-1}. \quad (6)$$

4. TM production at DAΦNE

Existing proposals for TM observation using resonant interactions involve the construction of an e^+e^- collider with a very large crossing angle $\theta \sim 30°$ so that TM has enough boost to allow the observation of its 1S decay vertex without requiring impractically small uncertainties on vertex and interaction point positions [13, 14].

In the following it will be shown instead that, by relaxing the requirement to observe the fundamental state and limiting to the study of excited states, TM can be discovered at 5σ at existing e^+e^- colliders, such as DAΦNE in Frascati [15], if running at the proper center-of-mass energy. It is indeed possible to exploit its non-zero crossing angle and provide enough boost to TM excited states, therefore observing their decay vertices and discriminating the signal over the background. It will be shown that, by running DAΦNE at a center-of-mass energy equal to $\sqrt{s} = 2m_\mu = 211.4$ MeV, the discovery of TM excited states with significance exceeding 5σ is possible with one month of data taking, using a cylindrical detector interface that embeds a multi-layer silicon tracker, a high-granularity electromagnetic calorimeter and a cosmic ray veto.

The technical difficulties of operating DAΦNE or other colliders with 105.7 MeV beams are beyond the scope of this article. As a proof-of-concept, a hypothetical discovery experiment using DAΦNE machine parameters will be described. The use of the DAΦNE collider as a benchmark for TM production is reasonable considering that, currently in the world, there is no other e^+e^- machines operating at such low energies. It should also be highlighted that the performances of the DAΦNE collider employed in the following are the ones delivered to the KLOE-II experiment at the nominal center-of-mass energy of 1020 MeV. Moreover, the details of the beam pipe and the interaction chamber will be also taken from the ones of the KLOE-II experiment at DAΦNE [16].

With a relative beam energy spread of 2×10^{-3} [17], the p-factor from equation (6) is 1.85×10^{-3}, leading to a realistic production cross-section of:

$$\sigma^{\text{real}}_{\text{ON } R.} \sim 124 \text{ pb}$$

therefore, with a daily luminosity of $10\,\text{pb}^{-1}\,\text{d}^{-1}$ [18], ∼1240 TM atoms are produced per day.

Note also that with here described resonant interactions, the TM is created in the spin 1 state, because its production is mediated by a virtual hard photon in the s channel, so it decays mostly to e^+e^- [12].

The DAΦNE crossing angle between the electron and positron beams is $\theta = 50$ mrad, thus producing a boost in the radial x direction [18]. The TM boost in x is then $m_\mu \sin\theta = 5.3$ MeV, hence $\beta_x\gamma = 2.5 \times 10^{-2}$, resulting in the average path lengths of TM states shown in table 1. The fluctuation of the boost in the Z direction is $\sqrt{2}\,m_\mu\sigma_E/E \sim 300$ keV, about 18 times less than the nominal boost in x, so it is safe to assume that the TM only moves in the x direction.

The path length values in the table should be compared to the interaction point x position uncertainty σ_X, where $(\sigma_X, \sigma_Y, \sigma_Z) = (200\ \mu\text{m}, 2.6\ \mu\text{m}, 20\ \text{mm})$ [18].

Table 1. Relative yield, lifetime and average path length (assuming $\beta\gamma = 2.5 \times 10^{-2}$) for TM spin 1 states, as a function of n.

n	Relative yield	τ_n [ps]	l_n [μ m]
1	0.833 33	1.8	13.6
2	0.104 17	14.5	108.4
3	0.030 86	48.8	366.0
4	0.013 02	115.7	867.6
5	0.006 67	225.9	1694.4
6	0.003 86	390.4	2928.0
7	0.002 43	619.9	4649.6
8	0.001 63	925.4	6940.4
9	0.001 14	1317.6	9882.0
10	0.000 83	1807.4	13 555.6

4.1. Initial state radiation

The effects of initial state radiation (ISR) on TM production should be carefully evaluated. On the one hand, the center of mass energy for the hard, partonic collision is reduced by radiation, which leads to a reduction in the cross section for the production of TM. On the other hand it boosts the electron pair, resulting in a boost of the intermediate TM.

To address the first effect the partonic cross section for producing TM is assumed to be constant and equal to equation (4) within the window $[2m_\mu - \Delta E,\ 2m_\mu]$, while it goes to zero outside this range. Then if $\mathcal{G}_{\mathrm{BES}}(s)$ is the Gaussian function describing the beam energy spread and $f_{\mathrm{ISR}}(x; s)$ is the radiator function, expressing the probability of an initial electron pair to carry a fraction x of the center of mass energy (see appendix B), the effective cross-section reads

$$\sigma_{\mathrm{TM,eff.}} = \int \mathrm{d}s'\ \mathcal{G}_{\mathrm{BES}}(s') \int \mathrm{d}x\, f_{\mathrm{ISR}}(x;\ s')\sigma_{\mathrm{TM}}(x^2 s'), \tag{7}$$

where the x integral is evaluated with the following extrema:

$$x_{\mathrm{min}}(s') = \min\left[1,\ \frac{2m_\mu - \Delta E}{\sqrt{s'}}\right] \tag{8}$$

$$x_{\mathrm{max}}(s') = \min\left[1,\ \frac{2m_\mu}{\sqrt{s'}}\right]. \tag{9}$$

By evaluating the integral numerically, a $\sigma_{\mathrm{TM,eff.}}$ of 93.9 pb is obtained.

Concerning the TM, random values of the energy of each collision were extracted according to the beam energy spread distribution and then the probability that, after ISR, the partonic center of mass energy is within the TM production window, was computed as

$$\int_{x_{\mathrm{min}}(s')}^{x_{\mathrm{max}}(s')} \mathrm{d}x f_{\mathrm{ISR}}(x;\ s'). \tag{10}$$

A distribution of the energy carried away by ISR, which can be approximated to the energy of a single ISR photon, is then obtained and shown in figure 2.

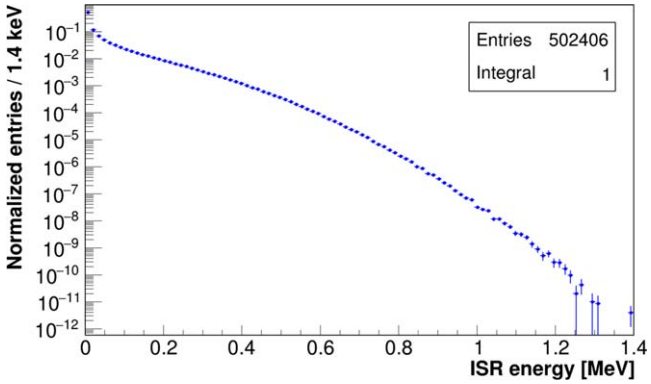

Figure 2. Distribution of energy radiated away by ISR for True muonium production.

5. Backgrounds discussion

At a center-of-mass energy of $\sqrt{s} = 2m_\mu \sim 211.4$ MeV, the only particles that can be produced are electrons, photons, single neutral pions, and muon pairs. Charged pions are excluded because there is not enough invariant mass available to produce a pair. A single charged pion must indeed be accompanied by a single electron to conserve charge, thus violating the lepton number conservation. Note that none of the remaining particles have lifetimes comparable with the one of TM, because electrons and photons are stable, neutral pions decay in 8.5×10^{-17} s, and muons, that never decay to e^+e^-, have a lifetime of 2.2 μs. Therefore, any displaced decay vertex in e^+e^- is a sign of TM presence, meaning that the only background is given by fake e^+e^- displaced vertices, due to particle mis-identification or to the finite resolution on the reconstructed vertex position. A detailed discussion of the backgrounds will follow.

5.1. Bhabha scattering

The dominant background is represented by Bhabha scattering, whose yield is several orders of magnitudes above the signal. Bhabha scattering produces electron pairs with the same energy as TM decay products, and it must be suppressed with appropriate cuts based on decay vertex and tracks reconstruction, in particular the tracks polar angle.

The differential Bhabha scattering cross section, at lowest order, is:

$$\frac{\mathrm{d}\sigma}{\mathrm{d}\Omega} = \frac{\alpha^2}{2s}\left[\frac{1+\cos^4(\theta/2)}{\sin^4(\theta/2)} - \frac{2\cos^4(\theta/2)}{\sin^2(\theta/2)} + \frac{1+\cos^2(\theta)}{2}\right] \tag{11}$$

Electron pairs originating from Bhabha scattering thus have predominantly small θ angles, while TM decay products are distributed as $\frac{\mathrm{d}N}{\mathrm{d}\cos\theta} \propto (1+\cos^2\theta)$ (neglecting the effect of the small TM boost). Therefore, an angular cut $[\theta_c, \pi - \theta_c]$ can be efficiently used to partly discriminate signal over background, using the asymptotic significance [19]:

$$Z(\theta_c) = \frac{\sigma_{\mathrm{TM}}(\theta_c < \theta < \pi - \theta_c)}{\sqrt{\sigma_{\mathrm{Bhabha}}(\theta_c < \theta < \pi - \theta_c)}}, \tag{12}$$

shown in figure 3, as a figure of merit. The shape of $Z(\theta_c)$ does not change if the signal or background yields are modified by other cuts independent from θ_c, so its maximum can be used to establish the optimal angular cut. As a trade-off between such optimization

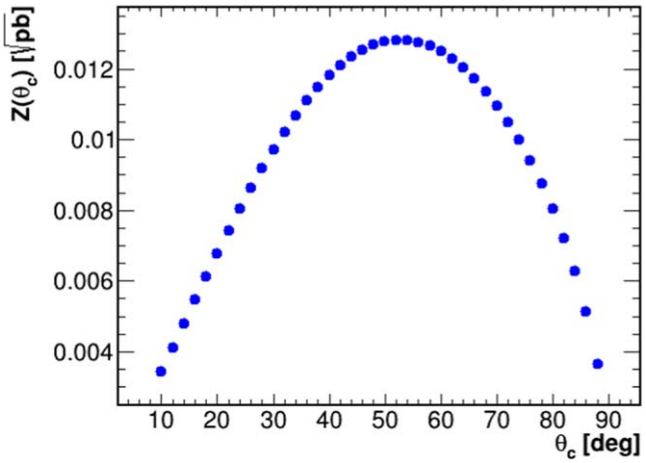

Figure 3. Significance scan in detector acceptance angle θ_c, at 1° steps (see equation (12)). The peak is around 53°.

($\theta^c_{\rm opt} = 53^\circ$) and a feasible detector geometry an angular cut of $\theta_c = 60^\circ$ is applied, therefore the TM production cross section reduces to $\sigma^{\rm real}_{\rm ON\,R.}(\theta_c = 60^\circ) \sim 39$ pb (taking ISR into account), corresponding to 390 TM/day at $10\,{\rm pb}^{-1}\,{\rm d}^{-1}$, while the Bhabha cross section at lowest order is $\sigma_{\rm Bhabha}(\theta_c = 60^\circ) \sim 9.35\ \mu$b.

This angular cut is not enough to efficiently suppress the Bhabha scattering background, hence other cuts based on tracks and vertex reconstruction are necessary. The precision on tracks reconstruction could be compromised by the multiple Coulombian scattering in the interaction region, that for this case (as in the KLOE-II experiment) is composed by a 50 μm thick beryllium beam pipe, surrounded by a 500 μm thick AlBeMet spherical vacuum chamber vessel [20]. In order to completely avoid the multiple Coulombian scattering in the vacuum chamber wall, the multi-layer silicon tracker must be installed around the beam pipe and inside the vacuum chamber.

In the following, it will be shown how a mitigation strategy is able to reject the Bhabha scattering events with an analysis based on reconstructed vertex position and the so-called line of response (LOR), derived from the positron emission tomography [21].

A proof-of-concept simulation was performed to understand the response to Bhabha scattering events at $\sqrt{s} = 2m_\mu$ of a cylindrical multi-layer silicon tracker with 100 μm thick layers (here only 2 for simplicity) and 10 μm spatial resolution. The simulation geometry embeds:

- the cylindrical 50 μm thick beryllium beam pipe placed at a 4.4 cm radius,
- a cylindrical 100 μm thick silicon layer placed at a 5 cm radius,
- a second cylindrical silicon layer at a 7 cm radius,

and its physical model takes into account:

- a 10 μm spatial resolution on both $r\phi$ and z,
- the multiple Coulombian scattering in all materials,
- the boost due to the non-zero crossing angle,
- uncertainties on the interaction point,
- the beam energy spread.

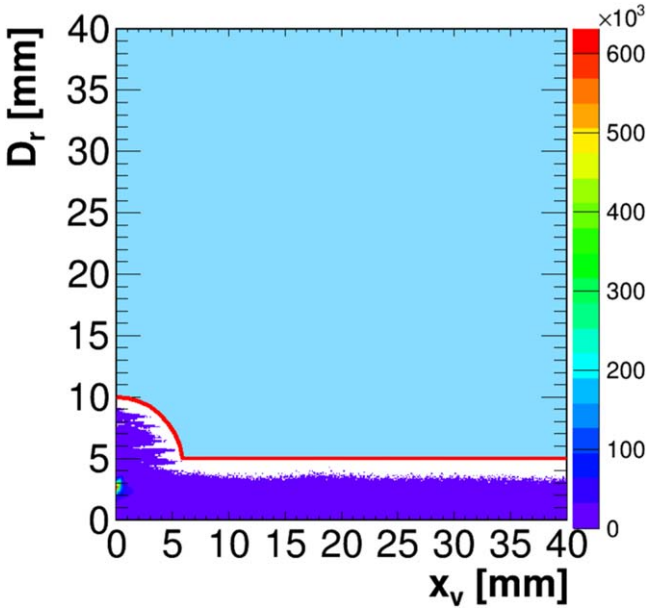

Figure 4. Joint distribution of D_r and x_v for 5×10^9 Bhabha scattering events, after the cut on α. The cuts $D_r > 5$ mm and the circular one are represented in red, and the signal region is filled in cyan.

For each event, the vertex position is reconstructed as the midpoint of the two closest approach points of the lines extrapolated from tracks hits in the silicon layer. As explained before, an additional quantity, D_r, is calculated, representing the distance between the beamline and the LOR connecting the two hits from the e^+ and e^- tracks in the first silicon layer. Using parallel computing, about $N_{\text{Bhabha}} = 5 \times 10^9$ Bhabha scattering events, including the emission of photons, were simulated using BabaYaga@NLO [22], a proper next-to-leading order event generator, and reconstructed as described above. The Bhabha scattering cross section was re-evaluated via BabaYaga@NLO, getting 9.0 μb, so it was only sligthly modified with respect to the value obtained at the leading order with the same angular cut. Given that the emission of hard photons makes the angle between the charged tracks smaller, a cut $\alpha > 177°$ on the opening angle between the electron and the positron has been applied. Indeed, the signal has a minimum opening angle of $\alpha = 2\sin^{-1}\frac{m_{\text{TM}}}{\sqrt{m_{\text{TM}}^2 + p_x^2}} = 177.13°$, where $p_x = 5.3$ MeV is the TM momentum (see section 4), therefore the signal efficiency of this cut is approximately 1. The joint distribution of D_r and x_v after the cut on α is shown in figure 4. By applying a cut $D_r > 5$ mm and a circular cut with the formula:

$$\sqrt{(D_r - 4\text{ mm})^2 + x_v^2} > 6\text{ mm} \tag{13}$$

no event is left in the signal region from the distribution in figure 4.

The probability that a Bhabha scattering event enters the signal region is then less than $1/N_{\text{Bhabha}} = 2 \times 10^{-10}$. With the three cuts sketched above ($\alpha > 177°$, $D_r > 5$ mm, and the circular one) the background from Bhabha scattering events is reduced to 0.54 events per month.

Note that, in a fraction of radiative Bhabha scattering events, the x_v and D_r based background rejection can be worsened, if the emitted photons interact before or inside the silicon

tracker. Photons not collinear to one of the tracks are generally vetoed by the calorimeter, while collinear photons interacting before it can be rejected by using a multi-layer silicon tracker embedding highly granular pixel sensors, featuring a spatial resolution of $\sim$10 μm. The tracker can indeed discriminate, by geometrically distinguishing the associated hits, the passage of electrons produced by Compton scattering, or e^+e^- pairs created by photon conversions, in addition to the two original back-to-back charged tracks.

A proper detector design, optimizing for instance the number of layers and the distances between them, would suppress this type of events at small enough levels to not sensibly affect the background yield.

Note that, even without complete simulations, it is understandable that, in the collinear approximation, photons conversions in the beam pipe or in the first silicon layer can be easily rejected. The opening angle of e^+e^- pairs from γ conversions at 100 MeV (worst case) is 14 mrad on average [23], which, in the case of a 2cm distance between the conversion point and the final silicon layer, translates in a $\sim$280 μm distance between the hits, much larger than the required $\sim$10 μm spatial resolution.

5.2. Other backgrounds

Other minor backgrounds should also be taken into account. They can easily be suppressed to small levels ($O(10^{-1})$ expected events in one month) using a proper detector design. Indeed, the most probable processes at $\sqrt{s} = 211.4$ MeV, excluding TM production and Bhabha scattering are:

- $e^+e^- \to \gamma\gamma$, $e^+e^- \to \gamma\gamma\gamma$
- $e^+e^- \to \mu^+\mu^-$
- $e^+e^- \to \pi^0\gamma$, $e^+e^- \to \pi^0 e^+e^-$

An additional background, not linked to e^+e^- interactions, is given by cosmic rays.

5.2.1. Annihilation into gamma rays. Annihilations in two or three gamma rays are very frequent at low-energy e^+e^- colliders. Pair annihilation into two gamma rays (with a soft cut-off of 10 MeV on the energy of other undetected photons) has indeed a large cross-section of 5.8 μb, with the $60° < \theta < 120°$ angular cut already discussed [24].

Photon interactions at 100 MeV can produce charged tracks that could fake electrons or positrons from signal events, when detected by both the calorimeter and all silicon layers. If only one photon interacts in the beam pipe or in the tracker, the calorimeter cluster from the other back-to-back photon does not have any track to match, so this type events would be rejected. A signal event can instead be faked if both photons interact, through pair production or Compton scattering (with a $Z \times 7.8$ mb cross section [25]), in the 50 μm thick beryllium beam pipe or in the first 100 μm thick silicon layer and only one electron/positron per photon is detected before the calorimeter. Concerning this type of events, photons undergoing conversions, accompanied by either conversion or Compton scattering of the other photon, can be suppressed at negligible levels using the same technique treated for the radiative Bhabha scattering case (see section 5.2). On the other hand, when both photons, with energy $E_\gamma \sim m_\mu$, undergo Compton scattering ($\sim$10 events/month), suppression strategies based on energy and vertex position discrimination can be applied. If a cut at 90 MeV is applied, assuming an energy resolution of $2\%/\sqrt{E_{\mathrm{GeV}}}$ (6% at 100 MeV), the signal efficiency is 99.4% and this background is rejected only by a factor $\sim$3.8, using the Klein–Nishina formula. For the events passing the energy selection, the electron is emitted mainly at small angles with respect to the primary photon, as shown in figure 5.

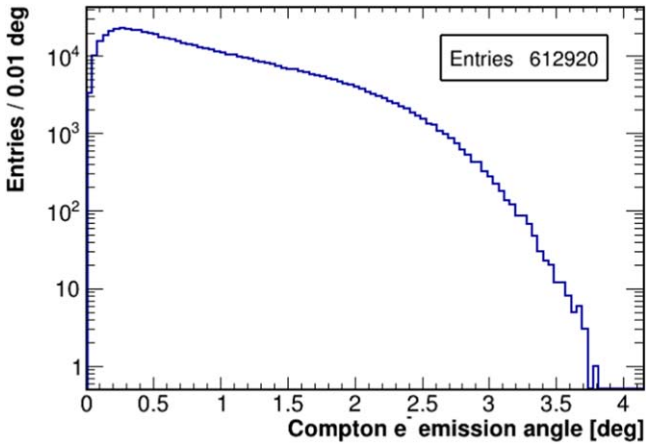

Figure 5. Distribution of the Compton electron emission angle with respect to the primary photon, for $E_\gamma = m_\mu$. Only electrons passing the cut on reconstructed energy $E > 90$ MeV, starting from 10^6 total events, are included in the histogram.

A displaced vertex can be faked only if the electrons are co-planar. Then, given that the electrons' emission angles are over $\psi = 3.5°$ with a probability of only $O(10^{-5})$ (see figure 5), in most cases the maximum distance of any fake displaced vertex from the beam axis is $R \sin\psi \sim 3$ mm, where $R \sim 5$ cm is the radius of the first silicon layer. Then, by employing a minimum cut on the displaced vertex position at 3 mm, the background from $e^+e^- \to \gamma\gamma$ is suppressed to negligible levels.

Pair annihilation into three gamma rays with energies E_{γ_i} has a cross section of [26]:

$$\sigma^{3\gamma}\left(E_{\gamma_i} > k\frac{\sqrt{s}}{2}\right) = \frac{2\alpha^3}{s}\left[3 - \frac{2\pi^2}{3} - (\ln 4\gamma^2 - 1)^2(2\ln k + 1)\right] \tag{14}$$

where k is the relative soft cut-off for all three photons and $\gamma = \frac{\sqrt{s}}{2m_e}$. With $k = 0.1$ ($\sim$10 MeV cut-off), the resulting cross section is 3 μb. When two photons are collinear and the calorimeter sees two clusters with reconstructed energy greater than 90 MeV, as in the two-photons case, the only non-negligible background is due to double Compton scattering. Indeed, when at least one γ conversion occurs, the event is rejected as for radiative Bhabha scattering, while the remaining case, i.e. triple Compton scattering, not only has a negligible yield but can also be discarded easily by distinguishing the three electron tracks.

In the case of double Compton scattering, the isolated photon has indeed reconstructed energy over 90 MeV, therefore the emitted electron angle is mostly contained in the 3.5° range as before, while the other photon undergoing Compton scattering can also have smaller energy and produce electrons at wider angles. An angular cut on the opening angle $\alpha > 177°$ between the two tracks, as reconstructed by the silicon detector, is applied (see section 5.2), therefore the sum of electrons emission angle is bounded under 3°, in the hypothesis that one electron is emitted clockwise and the other counterclockwise. A displaced vertex cannot be geometrically faked, indeed, if both electrons are emitted clockwise, or vice versa. After the cut $\alpha > 177°$, the annihilation in three photons can be treated as the two photons case, therefore its background yield is negligible.

A more quantitative study of the two and three-photon background, particularly from the point of view of the tracker response, requires full detector simulations which are outside the scope of this article.

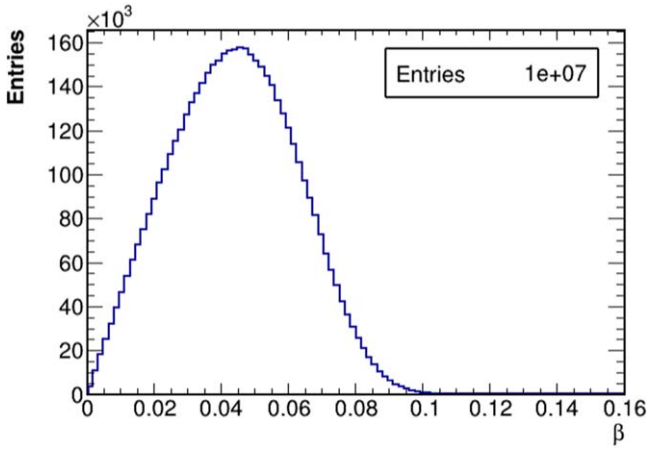

Figure 6. Muons β from simulation.

5.2.2. Muon pair production. Muon pair production takes place about the threshold, with cross section given by [12]

$$\sigma(e^+e^- \to \mu^+\mu^-) = \frac{2\pi\alpha^2\beta(3-\beta^2)}{3s}S(\beta), \tag{15}$$

where the Sommerfeld–Sakharov–Schwinger [27–29] enhancement factor

$$S(\beta) = \frac{X(\beta)}{1-e^{-X(\beta)}} \quad \text{with} \quad X(\beta) = \frac{\pi\alpha}{\beta}\sqrt{1-\beta^2} \tag{16}$$

has been included. In the above, $\beta = \sqrt{1-\frac{4m_\mu^2}{s}}$ is the speed (divided by c) of the outgoing muons [30]. The muons are produced only when $\sqrt{s} > 2m_\mu$, so it must be taken into account the beam energy spread ($\sigma_E/E \sim 2\times10^{-3}$) [17]. The cross-section can then be evaluated by simulation, extracting random values of $\sqrt{s}$ from a Gaussian distribution centered on $2m_\mu$ with a $\sigma_{\sqrt{s}} = 300$ keV, and calculating the resulting values of β, as seen in figure 6.

The average cross-section (without angular cuts) is evaluated to be 164 nb, which is about 3000 times higher than the 62 pb cross-section for TM production but about 100 times less than Bhabha scattering.

The produced muons have a kinetic energy of less than a few MeV, so they decay inside the beam pipe material or the tracker, and their energy deposit in the calorimeter is due to the Michel electron from the decay, or to photons from radiative muon captures, for μ^- only.

Positive muons can only decay freely, dominantly via the Michel [31] mode $\mu \to e + \nu_\mu + \bar{\nu_e}$, having a kinematic endpoint for the outgoing electron of $E_{max} = (m_\mu^2 + m_e^2)/(2m_\mu) = 52.8$ MeV, with a spectrum parametrized as follows:

$$\frac{d\Gamma}{dx} \propto 3x^2 - 2x^3 \tag{17}$$

where $x = E/E_{\max}$.

These electrons can be suppressed at negligible levels with the same calorimetric energy cut at 90 MeV employed for the two-photons case (see section 5.2.1).

5.2.3. Neutral pion production. The reaction $e^+e^- \to \pi^0\gamma$ has a cross-section of [32]:

$$\sigma(e^+e^- \to \pi^0\gamma) = \frac{8\,\alpha\,\Gamma_{\pi^0\to\gamma\gamma}}{3m_{\pi^0}^3}\left(1 - \frac{m_{\pi^0}^2}{s}\right)^3 \tag{18}$$

which corresponds to a value of 5 pb. There are three emitted photons (one as a recoil photon and two from π^0 decay) so this background is suppressed to negligible levels as in the three-photons case.

Another process producing neutral pions is $e^+e^- \to \pi^0 e^+e^-$, via photon-photon fusion, with a cross-section of 22 pb [32]. If the calorimeter detects four (two photons from π^0 decay and an electron–positron pair) or three different clusters, the events are directly discarded. If only two clusters are detected, because the photons from π^0 are emitted back-to-back and are collinear with electron or positron tracks, two situations must be distinguished. If there are photon interactions before the calorimeter, the technique treated for radiative Bhabha scattering (see section 5.2) can be applied to partially suppress this type of events. Otherwise, in the case of uninteracting or undetected photons, it is possible to see only two tracks in the silicon detector associated with two clusters in the calorimeter with energy compatible with $\sqrt{s}/2$, so this background is simply treated as very small contamination to Bhabha scattering, with a relative yield less than the ratio of the $e^+e^- \to \pi^0 e^+e^-$ to the Bhabha scattering cross section: $\sim 22\,\text{pb}/9\,\mu\text{b} = 2.5 \times 10^{-6}$.

5.2.4. Cosmic rays. Cosmic ray events can fake a signal event when they are not rejected by the calorimeter using cluster shapes or energy information. In the region inside the first silicon layer (with a radius of 5 cm), the number of cosmic ray events expected in one month is $O(10^7)$, assuming a 20 cm cylinder length.

This background can be rejected using a longitudinally segmented and high granularity crystals calorimeter. A possible solution is a cylindrical barrel calorimeter around the beam pipe as the one proposed for the future Muon Collider, Crilin [33, 34], with LYSO crystals and SiPM photo-sensors readout. Cluster shape and deposited energy analysis allows clear discrimination between cosmic rays and back-to-back e^+e^- pairs coming from beam interactions. This kind of calorimeter design allows discrimination between electron clusters and cosmic ray tracks, based on cluster shape, deposited energy topology, and time-of-flight characteristics. Hence, high muon rejection can be achieved by exploiting the high granularity, segmentation, and excellent timing capabilities. In order to increase the calorimeter discrimination factor by about 4 orders of magnitude, a hermetic cosmic ray veto detector surrounding the calorimeter can be built, leading to an expected number of cosmic rays events to be kept within 10^{-1} in one month.

6. Energy scan and off-peak measurements

By performing dedicated measurements in off-signal regions, for $\sqrt{s}$ above and below the TM mass, a data-driven characterization and subtraction of the expected background can be carried out, with a focus on the evaluation of the machine background. Indeed, although the machine parameters were extrapolated from DAΦNE performances at nominal energy, a complete simulation of the interaction zone is lacking, as it is the determination of the beam background. As a result, the aforementioned data-driven solution can conservatively provide a good indication of the background contamination at the TM $\sqrt{s}$, assuming that the continuum background distribution near the TM peak is flat.

Furthermore, dedicated energy scans around the $\mu^+\mu^-$ production threshold ($2m_\mu = 211.4$ MeV), can provide an absolute indication of the center-of-mass (CM) energy, against the sharp increase in $\mu^+\mu^-$ production, which can be evaluated based on the reconstruction of the previously described Michel spectra for electrons from muon decays.

7. Discovery potential

The number of background events expected in one month of data-taking has two main contributes: (1) the Bhabha scattering which can be suppressed using analysis cuts, and (2) the cosmic rays events that are independent on D_r and x_v, corresponding to less than 0.64 events/month.

The number of signal events has been estimated with the same detector simulation used for Bhabha scattering, and the secondary vertex has been simulated with contributions from all excited states. In order to achieve an effective signal/background discrimination, the following selection is required:

- Pre-selection cuts:
  - two reconstructed tracks with associated clusters in the calorimeter;
  - two calorimeter clusters with an energy greater than 90 MeV (see section 5.2.1);
  - two and only two opposite charged particles detected in all silicon layers (see section 5.2);
  - opening angle greater than 177° (see section 5.2.1);
  - vertex x_v coordinate less than 40 mm
  - $D_r < 44$ mm
- Analysis cuts:
  - Circular cut (see equation (13)): required events out of the circle with center (0 mm, 4 mm) with 6 mm radius in the plane (x_v, D_r)
  - $D_r > 5$ mm

The joint distribution of D_r and x_v distribution for signal events, not including ISR effects, after pre-selection cuts, is shown in figure 7. The upper cuts on vertex x_v coordinate (40 mm) and D_r (44 mm) are due to the presence of the beam pipe at a radius of 44 mm.

The efficiency on the signal after pre-selection and analysis cuts is $(8.2 \pm 0.2) \times 10^{-3}$, without including ISR effects. As shown in figure 2, the 99.5% of the events includes an ISR emission with an energy lower than 400 keV. In order to roughly estimate the effect of ISR on the signal, the presence of an ISR photon with a 400 keV energy has been included for different values of the ISR photon polar angle and with uniformly distributed azimuthal angles, as shown in figure 8.

The efficiency of the signal can then be underestimated as 7.8×10^{-3}, looking at the lowest efficiency in figure 8. The expected number of signal events in 30 d of data-taking with a 10 pb^{-1} d luminosity and a 39 pb cross section is then greater than 91. Given that the expected number of background events is less than 0.64, the significance is greater than 27σ, greatly exceeding the conventional 5σ threshold for discovery. It has been also established that, with the same cuts and the same data-taking time, a discovery can be achieved with luminosity values as low as 0.5 pb^{-1} d, as the expected number of signal events, background from cosmic rays and Bhabha scattering are, respectively, 4.6, 0.1 (unvaried) and 0.03.

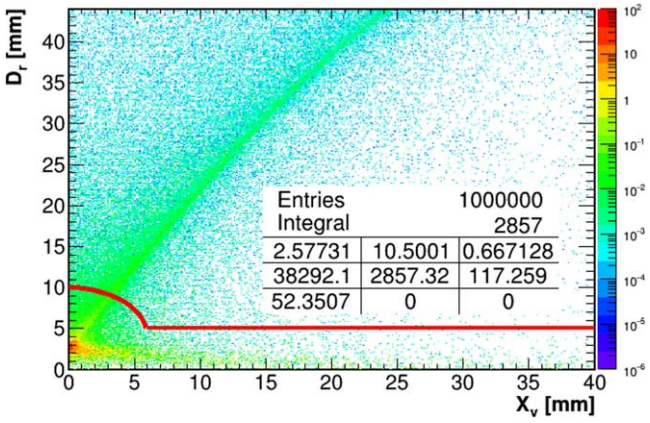

Figure 7. 2D distribution of x_v and D_r for signal events. The red lines represent the analysis cuts (see figure 4).

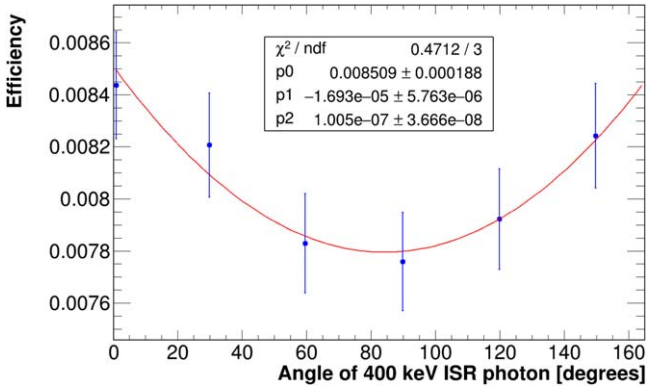

Figure 8. Efficiency of the signal including a 400 keV ISR photon for all the events with different polar angles. The values have been fitted with a parabola to extract the minimum value.

8. TM spectroscopy

As already mentioned, one of the motivations for the study of TM is its potential in probing BSM physics or precision SM physics, and especially in shedding new light on the long-standing muon $g-2$ (a_μ) problem. Indeed, precise measurements of the properties of TM (hyper-fine splittings, Lamb shift) can be used in combination with measurements of a_μ to probe several BSM scenarios in which the new physics couples to muons [35], as they in general predict modifications of these properties, and also to estimate the contribution to $(g-2)_\mu$ from hadronic vacuum polarization [5]. As explained in the introduction, TM has a broad physics reach, due to the absence of large hadronic contributions and to the large reduced mass compared to positronium or muonium.

In an experimental phase subsequent to discovery, if a large enough number of TM bound states is available, the Lamb shift may be measured by means of a laser of appropriate frequency to excite the P states of TM. Focusing on the $n=2$ states, a laser frequency of

about 10 THz [2] would excite $2S$ states to $2P$, which, as discussed above, would then have to decay to $1S$ emitting x-rays in the keV range, so measuring the $2P \rightarrow 1S$ transitions x-ray yield as a function of the laser frequency provides an estimate of the Lamb shift. BSM contributions modify the Lamb shift frequency by $O(100)$ MHz, a value in the reach of modern spectroscopy techniques, therefore TM could be efficiently used as a BSM probe. Finally, it should be remembered that the measurement of the hydrogen atom Lamb shift was a milestone of modern physics, as it confirmed QED correctness, and that bound states spectroscopy, in general, provides very sensible probes.

9. Timeline estimate

It was shown in the previous sections that there is large enough discovery potential in already existing e^+e^- colliders, such as the DAΦNE one in Frascati, in order to reduce as much as possible costs and time requests. However, it is likely that, in order to change the beam energy, some modifications to the apparatus optics, acceleration sections and magnets might be needed. It comes unsaid that a time estimate for these modifications is strictly linked to the characteristics of the collider. Thus, it is quite difficult to provide a time estimate without a full dedicated machine study, which is beyond the scope of the article.

Regarding the experimental apparatus, instead, the requested detectors are of doable construction since they are all based on mature and well-known technologies, and it would require no more than one and an half year.

After this rough timeline estimate, the presence of possible competitive experimental proposals should be taken into account. As anticipated in section 1, besides $e^+e^- \rightarrow TM$, another feasible method for observing TM is the massive production of η mesons decaying into $TM\gamma$ [7]. This kind of production might be achievable in LHCb RunIII [8] at discovery levels. However, a discovery of TM by means of the LHCb experiment is actually compatible with the here presented experimental proposal. Indeed, not only it would confirm their discovery with a completely different approach but, thanks to its configuration, it would also allow to study the spectroscopy of TM bound states (section 8).

10. Conclusion

Several of BSM discovery potential is hidden in the atomic spectroscopy of QED-bound states. Among these interesting objects, one of the most sensible ones, is the so-called TM, a $\mu^+\mu^-$ bound state. TM can be produced on resonance with a 67 nb cross-section at e^+e^- collider running at a $2m_\mu = 211.4$ MeV center-of-mass energy.

In real-world scenarios, due to the smallness of its B.E. with respect to the beam's energy spread σ_E, the cross-section is smaller by a factor proportional to σ_E.

In this paper, the DAΦNE collider at the Frascati National Laboratory of INFN [36] is used, which now runs at $\sqrt{s} = 1020$ MeV, as the benchmark of machine requirements for TM research. For this reason, its beam and collision parameters were studied to assess whether there is a potential for discovery of TM excited states, in the hypothesis to run at the proper $\sqrt{s}$. The TM decay vertex to an electron pair can indeed be reconstructed and employed to discriminate signal over background. It was therefore shown that TM excited states can be observed in a data-taking of the order of one month using a detector with a polar acceptance angle of $\theta = 60°$, made of a multi-layer silicon tracker with 10 μm spatial resolution, a calorimeter with a resolution better than $2\%/\sqrt{E\,[\mathrm{GeV}]}$, and a hermetic cosmic ray veto.

Previous proposals for TM discovery involved the construction of e^+e^- colliders with large collision crossing angles ($\theta \sim 30°$), in order to provide TM with enough boost to observe its fundamental state [13]. On the contrary, it was proved that also the small crossing angle of already existing colliders like DAΦNE is sufficient to discover TM, by observing its excited states.

Acknowledgments

The authors are grateful to M.Raggi and S. Miscetti, for the careful reading of the paper and for valuable suggestions and comments. They also thank the whole Acceleration Division of the Laboratori Nazionali of Frascati for providing them with the DAΦNE beam parameters used in this paper and C. Carloni Calame for help with the Babayaga generator.

Data availability statement

No new data were created or analysed in this study.

Appendix A. Methods

The significance is calculated as:

$$Z = \sqrt{-2\log L(N,\,0)/L(N,\,1)} \tag{A1}$$

where $L(N,\,\mu)$ is the Poissonian likelihood with N observed events, a signal strength of μ (0 for background only, 1 for nominal signal yield), $s(b)$ expected signal (background) events [19]

$$L(n,\,\mu) = \frac{(\mu s + b)^N}{N!}\exp{-(\mu s + b)}. \tag{A2}$$

Appendix B. Initial state radiation

The ISR radiator function used in equation (7) and equation (10) is essentially the probability that the electron pair carries a given fraction of the nominal center of mass energy. The following relations were used: [37–39]

$$f_{\rm ISR}\,(x;\,s) = f^0_{\rm ISR}\,(x;\,s)\left(1 + \frac{\beta_l}{2} - \frac{1}{2}(1 - x^2)\right), \tag{B1}$$

where $\beta_l = \frac{2\alpha}{\pi}\left(\log\frac{s}{m_e} - 1\right)$, and

$$f^0_{\rm ISR}\,(x;\,s) = \frac{\exp\left(\frac{\beta_l}{4} + \frac{\alpha}{\pi}\left(\frac{1}{2} + \frac{\pi^2}{3}\right) - \gamma_E\beta_l\right)}{\Gamma(1 + \beta_l)}\beta_l(1 - x)^{\beta_l - 1}. \tag{B2}$$

ORCID iDs

Ruben Gargiulo https://orcid.org/0000-0001-7202-881X

References

[1] Karshenboim S G 2004 Precision study of positronium: testing bound state QED theory *Int. J. Mod. Phys.* A **19** 3879
[2] Lamm H and Ji Y 2018 Predicting and discovering true muonium *EPJ Web Conf.* **181** 01016
[3] d'Enterria D and Shao H-S 2023 Prospects for ditauonium discovery at colliders *Phys. Lett.* B **842** 137960
[4] Kriewald J 2023 Muons: a gateway to new physics *Phys. Sci. Forum* **8** 28
[5] Lamm H 2017 Hadronic vacuum polarization in true muonium *Phys. Rev.* A **95** 012505
[6] Crivellin A, Hoferichter M, Manzari C A and Montull M 2020 Hadronic vacuum polarization: $(g-2)_\mu$ versus global electroweak fits *Phys. Rev. Lett.* **125**
[7] Ji Y and Lamm H 2019 Scouring meson decays for true muonium *Phys. Rev.* D **99** (3) 033008
[8] Vidal X C, Ilten P, Plews J, Shuve B and Soreq Y 2019 Discovering true muonium at LHCb *Phys. Rev.* D **100** 12053003
[9] Ji Y and Lamm H 2018 Discovering true muonium in $K_L \to (\mu^+\mu^-)\gamma$ *Phys. Rev.* D **98** 053008
[10] Holvik E and Olsen H A 1987 Creation of relativistic fermionium in collisions of electrons with atoms *Phys. Rev.* D **35** 2124
[11] Ginzburg I F, Jentschura U D, Karshenboim S G, Krauss F, Serbo V G and Soff G 1998 Production of bound mu+ mu- systems in relativistic heavy ion collisions *Phys. Rev.* C **58** 3565
[12] Brodsky S J and Lebed R F 2009 Production of the smallest qed atom: true muonium (mu+ mu−) *Phys. Rev. Lett.* **102** 213401
[13] Fox P J, Jindariani S and Shiltsev V 2023 Dimus: super-compact dimuonium spectroscopy collider at fermilab *JINST* **18** 8T08007
[14] Bogomyagkov A V, Druzhinin V P, Levichev E B, Mil'shtein A I and Sinyatkin S V 2018 Concept of an electron–positron collider for production and study of the $(\mu^+\mu^-)$ bound state *Phys. Part. Nucl. Lett.* **15** 740
[15] Vignola G and Team D P 1996 Dafne, the first phi-factory *5th European Particle Accelerator Conf., Sitges (Spain), Proc.* p 22
[16] Bencivenni G and the KLOE Collaboration 1999 The status of the kloe experiment *AIP Conference Proceedings* vol 459 (American Institute of Physics) pp 116–24
[17] Spadaro T Dafne beam energy spread in 2002 period of kloe data taking 2002 https://lnf.infn.it/kloe/private/bes2002.html
[18] Milardi C and D project team 2009 Present status of the daphne upgrade and perspectives *Int. J. Mod. Phys.* A **24** 360
[19] Gross E 2018 Practical statistics for high energy physics *CERN Yellow Rep. School Proc.* **3** 199
[20] Babusci D *et al* 2014 Test of cpt and lorentz symmetry in entangled neutral kaons with the kloe experiment *Phys. Lett.* B **730** 89
[21] Turkington T G 2001 Introduction to pet instrumentation *J. Nucl. Med. Technol.* **29** 4
[22] Balossini G, Carloni Calame C M, Montagna G, Nicrosini O and Piccinini F 2006 Matching perturbative and parton shower corrections to bhabha process at flavour factories *Nucl. Phys.* B **758** 227–53
[23] Olsen H 1963 Opening angles of electron–positron pairs *Phys. Rev.* **131** 406
[24] Berends F and Kleiss R 1981 Distributions for electron–positron annihilation into two and three photons *Nucl. Phys.* B **186** 22
[25] Habs D, Günther M M, Jentschel M and Urban W 2011 Refractive index of silicon at γ ray energies *Phys. Rev. Lett.* **108** 184802
[26] Lee R N 2020 Electron–positron annihilation to photons at o(α3) revisited *Nucl. Phys.* B **960** 115200
[27] Sommerfeld A 1939 *Atombau und Spektrallinien* (Braunschweig: Vieweg) 2nd edn vol 2
[28] Schwinger J S 1973 *Particles, Sources and Fields* (New York: Perseus Books) vol 2
[29] Sakharov A D 1948 Interaction of an electron and positron in pair production *Zh. Eksp. Teor. Fiz.* **18** 631
[30] Bystritskiy Y M, Kuraev E A, Fedotovich G V and Ignatov F V 2005 Cross sections of muon and charged pion pair production in electron–positron annihilation near the threshold *Phys. Rev.* D **72** 114019
[31] Muon decay parameters http://pdg.lbl.gov/2018/ reviews/rpp2018-rev-muon-decay-params.pdf (2013) [Online; accessed 19 October 2023]
[32] Chilton F 1961 Pion production in electron–positron collisions *Phys. Rev.* **123** 656

[33] Ceravolo S *et al* 2022 Crilin: a crystal calorimeter with longitudinal information for a future muon collider *J. Instrum.* **17** P09033
[34] Cantone C *et al* 2023 Beamtest, simulation, and performance evaluation of pbf2 and pwo-uf crystals with sipm readout for a semi-homogeneous calorimeter prototype with longitudinal segmentation *Frontiers* **11** 1
[35] Cid Vidal X, Ilten P, Plews J, Shuve B and Soreq Y 2019 Discovering true muonium at LHCb *Phys. Rev.* D **100** 053003
[36] Gianotti P 2020 The research activity of the frascati laboratory *J. Instrum.* **15** C06047
[37] Greco M, Han T and Liu Z 2016 Isr effects for resonant higgs production at future lepton colliders *Phys. Lett.* B **763** 409–15
[38] Jadach S and Kycia R 2016 Lineshape of the higgs boson in future lepton colliders *Phys. Lett.* B **755** 58–63
[39] Jadach S, Ward B F L and Was Z 2001 Coherent exclusive exponentiation for precision monte carlo calculations *Phys. Rev.* D **63** 113009